ORIGINAL PAPER

Influence of individual cell motility on the 2D front roughness dynamics of tumour cell colonies

N. E. Muzzio · M. A. Pasquale · P. H. González · A. J. Arvia

Abstract The dynamics of in situ 2D HeLa cell quasi-linear and quasi-radial colony fronts in a standard culture medium is investigated. For quasi-radial colonies, as the cell population increased, a kinetic transition from an exponential to a constant front average velocity regime was observed. Special attention was paid to individual cell motility evolution under constant average colony front velocity looking for its impact on the dynamics of the 2D colony front roughness. From the directionalities and velocity components of cell trajectories in colonies with different cell populations, the influence of both local cell density and cell crowding effects on individual cell motility was determined. The average dynamic behaviour of individual cells in the colony and its dependence on both local spatio-temporal heterogeneities and growth geometry suggested that cell motion undergoes under a concerted cell migration mechanism, in which both a limiting random walk-like and a limiting ballistic-like contribution were involved. These results were interesting to infer how biased cell trajectories influenced both the 2D colony spreading dynamics and the front roughness characteristics by local biased contributions to individual cell motion. These data are consistent with previous experimental and theoretical cell colony spreading data and provide additional evidence of the validity of the Kardar-Parisi-Zhang equation, within a certain range of time and colony front size, for describing the dynamics of 2D colony front roughness.

Keywords Cell population · Colony spatio-temporal heterogeneity · Crowding effects · Biased cell trajectories · Cell migration concerted mechanism

N. E. Muzzio · M. A. Pasquale (✉) · A. J. Arvia
Instituto de Investigaciones Fisicoquímicas Teóricas y Aplicadas (INIFTA), Universidad Nacional de La Plata (UNLP), CONICET, Sucursal 4, Casilla de Correo 16, 1900, La Plata, Argentina
e-mail: miguelp@inifta.unlp.edu.ar

P. H. González
Cátedra de Patología, Facultad de Ciencias Médicas, UNLP, CIC, Calle 60 y 120, 1900, La Plata, Bs. As., Argentina

1 Introduction

Cell motility plays an important role in tissue spreading in the normal functioning of organisms during growth and mature phases, such as wound healing [1, 2] and malignant tumour growth and metastasis [3–5]. Different aspects of individual cell motility and cell migration in colonies are relevant to deal with the dynamic behaviour of these biosystems [6–8] either for assisting or inhibiting their motility according to their spreading regimes [9]. Cell motility usually involves a drag on 2D or 3D extracellular environments, a process that mainly depends on substrate surface-cell and cell-cell interactions [10]. The spatio-temporal variation of these interactions is linked to changes in the degree of structural global heterogeneities, accompanying the colony spreading. These variations occur in conjunction with other processes of either biological or physical nature that influence individual cell motility and consequently, the colony spreading dynamics itself [11, 12].

Both cell adhesion and migration are strongly influenced by the extracellular matrix structure. For cells of similar origin and morphology, the concomitant influence of environmental signals on cell response also occurs, as appears to be the case of normal and cancerous cells [13]. However, multi-cellular collective migration implies physically and functionally continuous cell-cell connections, the multi-cellular polarity and supra-cellular organisation of the actin cytoskeleton for generating traction and protrusion forces maintaining cell-cell junctions, and the movement of cell groups structurally modifying the tissue along the migration path either by clearing the track or producing extracellular matrix modification, including the deposition of a basement membrane [14].

Different experimental techniques to obtain basic cell motility data in collective migration have been proposed. Among them, in vitro wound healing assays by scratching a cell monolayer [15], or peeling away a mask [16, 17] or generating a colony by seeding cells in a confined space and the sudden release of the constraints after cell attachment [18] have been utilised. The characteristics of this type of experiment were analysed employing Madin-Darby canine kidney (MDCK) cells and an engineered system that allowed the dissection of the classic scratching assay [16]. The growth of a non-uniform interface with a finger-like morphology involves cells in sub-marginal moving domains that extend lamellipodia towards the edges and crawl, instead of just moving passively, when cells at the margin pull on them [19].

Steady multi-cell migration data of epithelial cells from scratch wound assays were interpreted by a cell sheet migration agent model [20] in which cells are simple mechanical agents that sense when they are crowded and respond with lower division rates and migration towards a less crowded area, neglecting cohesive cell junctions. This model was tested with experiments on L1 fibroblasts.

The use of Fischer's equation has also been proposed to introduce inhibition effects [21, 22], as in a multi-scale model that has been presented to describe the colony behaviour at the cell population scale and at the individual cell scale, respectively [23]. The continuum model was based on the generalised Fischer's equation including migration contact inhibition, whereas the discrete model was derived from the former one employing master equations. These models were tested against 3T3 fibroblast culture data.

Another continuum model of cell macroscopic dynamics involving chemotaxis and direct contact interactions with microscopic limits [24] established a connection between a discrete stochastic model of fluctuating cells based on the Monte Carlo method and macroscopic equations describing cellular density dynamics. Cells with randomly fluctuating shapes are driven by chemical gradients and utilising the excluded volume approach, a non-linear diffusion equation from 1D and 2D microscopic dynamics has been derived. A

Monte Carlo-based growth kinetic model of a cell population in 2D and 3D space and an analytical approach to obtain the time evolution have also been presented [25].

The collective spreading of cells has also been linked to the variation of cell aspect ratios [26]. From a multi-scale approximation involving the collective motion of a population of interacting agents in a generalised lattice-based exclusion process, the following conclusions were derived: (i) for round agents that occupy a single lattice site, the behaviour of the biosystem can be described by a linear diffusion equation; (ii) for elongated rod-shaped agents that occupy a number of adjacent sites, the system can be represented by porous equation media. This approach provides a physical connection between the collective cell spreading, either (i) or (ii) and the agent shapes to represent cell density profiles.

The above survey of cell motility mechanisms for interpreting the collective spreading of confluent colonies of epithelial cells at the monolayer level suggested the possibility that the different transport of agents under either linear or non-linear conditions could also be studied from the characteristics of cell trajectories followed within time windows sufficiently small to avoid the influence of cell proliferation on colony spreading. For each constant composition biosystem, the prevailing mechanism would depend on the cell population, i.e., the colony age and on the spatio-temporal heterogeneities at the cell level (cell shape, size and orientation) and at the colony level (structure and density of cellular domains). These physical variables, which are intimately coupled with complex biological mechanisms, should play a key role in determining the equation describing the colony front displacement, its fractal dimension and the colony front roughness dynamics. The latter is usually evaluated utilising the dynamic scaling theory and Fourier transform analysis to obtain a set of roughness exponents that is compared to those predicted by different condensed phase growth models [27, 28]. Our recent results on the roughness front 2D spreading dynamics of HeLa cell colonies [29] showed that it was characterised by a set of roughness exponents similar to that predicted by the 1D Kardar-Parisi-Zhang (KPZ) equation for rough front displacements of condensed phases [30, 31], at least for a certain range of growth time and colony front length. This equation involves the contribution of a linear differential term (diffusion), a non-linear term (biased trajectories of agents) and a stochastic term. The investigation of cell trajectories becomes particularly interesting to support the contribution of the non-linear term.

This paper focuses on the collective cell migration of 2D spreading HeLa cell colonies. Collective cell migration in cancer cells has been less studied to date than morphogenesis and regeneration but there is strong evidence that collective invasion in cancer recapitulates key steps of morphogenic movement in a deregulated manner [14]. It describes different dynamic aspects of in situ 2D q-linear (QLC) and q-radial (QRC) colony fronts under constant environmental conditions. Cell tracking data were obtained from QLC at constant velocity regime and QRC with different initial cell populations under both exponential and constant front velocity regimes. These data provided information about individual cell trajectories and crowding effects and suggested that individual cell motility involved a concerted cell transport mechanism in which there are contributions from both a random walk-like and a ballistic-like motility. Their relative rate contribution depended on the cell population, the instantaneous, local heterogeneity of colony domains and the growth geometry resulting in biased cell trajectories that are compatible with the predictions of a KPZ growth model approach. The collective cell migration at the monolayer was consistent with the unifying principle recently stated, which established that in the transport process neighbouring cells join forces to transmit appreciable normal stress across cell-cell junctions but migrate along orientations of minimal intercellular shear stress [32, 33].

2 Experimental

2.1 Colony preparation procedures

HeLa cells, passage 44–60, were employed. Cell colonies were cultured on polystyrene Petri dishes 3.6 cm in diameter (Greiner bio-one), in RPMI medium supplemented with 10% FBS, 2 gl^{-1} bicarbonate and 100 M ml^{-1} streptomycin. The cultures were incubated in an oven at 37 °C in a 5% carbon dioxide and 97% humidity atmosphere. As required, half of the medium was changed every 2 days to maintain its composition practically constant. Cell viability was achieved by Trypan blue vital staining.

Each QRC was formed by seeding 2 ml of supplemented medium containing 1000–2000 cells into Petri dishes. Cells were allowed to adhere and grow for 4–5 days forming colonies with a different initial number of cells (N_0) at t_0, the time at which growth data collection was started. As these colonies are formed spontaneously after seeding without confinement, colony expansion data could be obtained immediately afterwards.

Each QLC was prepared as described elsewhere [34] utilising a sterilized Teflon® tape 2.2 cm wide and 100 μm thick to cover the central region of a Petri dish bottom. Subsequently, a suspension of about 20000 cell ml^{-1} in supplemented medium was seeded. Cell duplication formed colonies that spread on the remaining free surface of the Petri dish bottom. After about 2 days, the time required for reaching a confluent cell monolayer, the Teflon tape was removed. To avoid the influence of cell confinement, first spreading data from QLC were collected about 20 h after the Teflon tape had been removed.

2.2 Colony growth pattern micro-imaging

Colony growth patterns were imaged using a Nikon DS-Fi digital camera coupled to a Nikon TS100 phase-contrast inverted microscope with a CFI flat field ADL 10X objective. The image resolution was 1 μm = 2.1 pixel. The colony growth time (t) was counted from t_0.

In situ cell colony digital images were obtained by a time-lapse system at intervals in the range $5 \leq \Delta t' \leq 45$ min during 2–3 days. For this purpose, QRC with different N_0 and QLC were placed in a chamber that was fixed to the microscope platform and maintained at 37 °C and 97% humidity. Before placing each Petri dish in the chamber, the culture medium was changed to RPMI CO_2-Independent Medium (Gibco, Invitrogen Corp.) for preserving the pH. Occasionally, the culture medium was replaced by fresh RPMI bicarbonate supplemented medium under a 5% CO_2-air atmosphere. Both media contained L-glutamine and streptomycin.

2.3 Colony data processing

Images of QLC and QRC patterns were analysed as previously described [34, 35]. Briefly, colony fronts were manually traced using a Wacom graphic table. The trace error, evaluated from zoomed images of colony growth patterns, resulted in the order of 1 pixel. For data processing, an in-lab developed program was utilised. For QLC the instantaneous vertical distance from the horizontal origin line to the ith point at the front at time t ($h_i(t)$) ($i = 1$, 2, ...n) and the mean colony distance $\langle h \rangle = \sum_i h_i(t)/n$ were evaluated. Similarly, for QRC the colony centre of mass (CM), the instantaneous distance ($R_i(t)$) from CM to the ith point at the front and the mean colony radius $\langle R \rangle = \sum_i R_i(t)/n$ were determined.

2.4 Individual cell trajectories

Trajectories of selected cells were obtained from the instantaneous 2D coordinates ($\mathbf{P}_j = \mathbf{p}(t_i) = x_j(t_i), y(t_i), i = 1, 2, \ldots n$) by manually tracking time-lapse movie frames employing Image Pro Plus 6.0 software, Media Cybernetics Inc.

The location of CM at t_0, the distance from CM to each cell ($r_i(t)$) and the corresponding angle ($\Theta_i(t)$) were determined from QRC cell tracking data. Coordinate evaluations were obtained from either the position of the cell nucleus or the centroid of each drawn digital cell contour. From an average of 10 trajectories followed for about 24 h, the difference between both procedures was about 10%. The mean cell velocity $<V_i>$ was obtained from coordinate data according to:

$$\langle V_i \rangle = \frac{\mathbf{p}_j(t_{i+1}) - \mathbf{p}_j(t_i)}{\Delta t'}. \tag{1}$$

Velocity components parallel (V_{par}) and perpendicular (V_{per}) to the colony front were evaluated within the interval range $15 \leq \Delta t' \leq 45$ min. Despite the error of each cell nucleus location, for all values of $\Delta t'$ the same trajectory was obtained.

The mean square displacement (msd) was evaluated by the following equation:

$$msd = \left\langle \left((x_i(t_0 + \Delta t) - x_i(t_0))^2 \right) + \left((y_i(t_0 + \Delta t) - y_i(t_0))^2 \right) \right\rangle \tag{2}$$

where t_0 is the starting time of the recording interval (Δt). Average data from all values of t_0 and all cell trajectories were derived following reference [36, 37].

The msd dependence on Δt can be expressed by the power law:

$$\langle msd(\Delta t) \rangle \propto \Delta t^b \tag{3}$$

where the constant b is 1 for random walk displacement and 2 for ballistic motion [38].

For QRC ($N_0 < 20$ cells) all cells were tracked, whereas for QRC ($N_0 > 1000$ cells) only those cells initially located inside an outer colony stripe of a thickness equivalent to three cell average diameters were tracked. Cell tracking was performed over the range 720–4320 min.

3 Results

3.1 2D colony spreading kinetics

The colony spreading comprised different spatio-temporal scales depending on whether attention was paid to either the colony growth kinetics and roughness development or the individual cell motility. The average cell duplication constant was evaluated by following the evolution of those QRC patterns whose population (N) changed from $4 \leq N_0 \leq 100$ to $N = 1000$ cells, approximately, over about 15 days (Fig. 1). The 2D growth kinetics of these colonies, expressed in terms of the total number of cells at time t, fulfils the exponential relationship:

$$\frac{N}{N_0} = \exp(\langle k \rangle t) \tag{4}$$

where $<k>$, the average first-order rate constant, is the reciprocal of the average cell duplication time, i.e., $<k> = [<\tau>]^{-1}$. From the log (N/N_o) versus t plots (Fig. 2a) it follows that $<\tau> = 2400 \pm 400$ min.
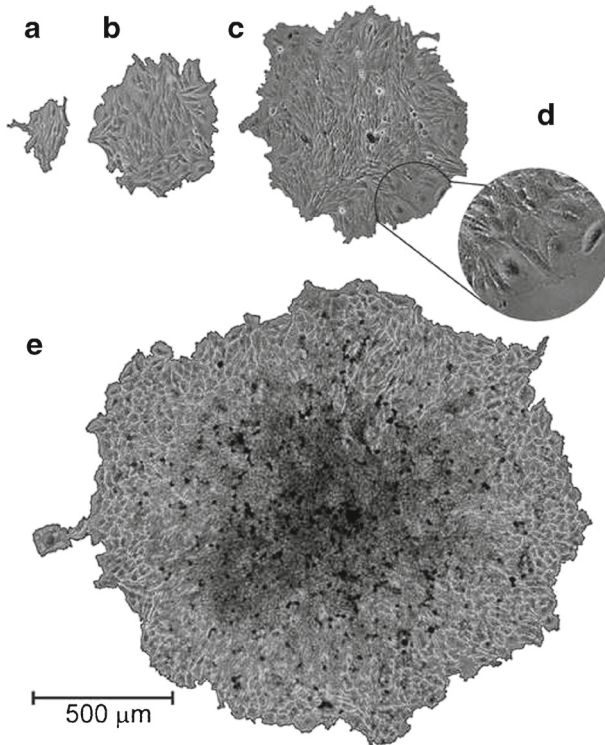
Fig. 1 HeLa cell QRC growth pattern sequence: **a** $t = 0$ min; **b** $t = 5612$ min; **c** $t = 9220$ min; **e** $t = 18130$ min. A zoomed region from the colony border **c** is depicted in **d**. 3D cell domains (*the darkest black spots*) at the inner region of the colony **e** can be seen

For QRC starting from low N_0 up to the initial formation of 3D domains, the same kinetic law either from N or $<R>$ was fulfilled (Fig. 2). But when $N > 1500$ cells, the 2D average front displacement velocity ($<V_f>$) gradually changed from an exponential to a constant $<V_f>$ kinetic regime (Figs. 2a and 3).

On the other hand, data from QRC ($N_0 > 1500$ cells) and QLC [29] attained the value $<V_f> = 0.09 \pm 0.05$ μm min^{-1} in a short time, at least for the time scale of these experiments (Fig. 2a and b).

### 3.2 Morphology changes from colony growth patterns

Sequential 2D growth patterns showed a number of morphology features that depended on N. Thus, QRC ($4 \leq N \leq 500$ cells) initially displayed irregular 2D fronts and progressively tended to quasi-circular forms. Furthermore, the average size and shape of cells remained rather uniform and the average cell-cell distance became relatively larger than for greater N. Conversely, from $N > 1500$ cells, as the constant $<V_f>$ regime was attained (Fig. 3), the growth patterns displayed spatio-temporal-dependent heterogeneities resulting from changes in cell size distribution and cell morphology. Then, the cell-cell average distance diminished from the outer to the inner colony region [29] and quasi-ordered 2D cell
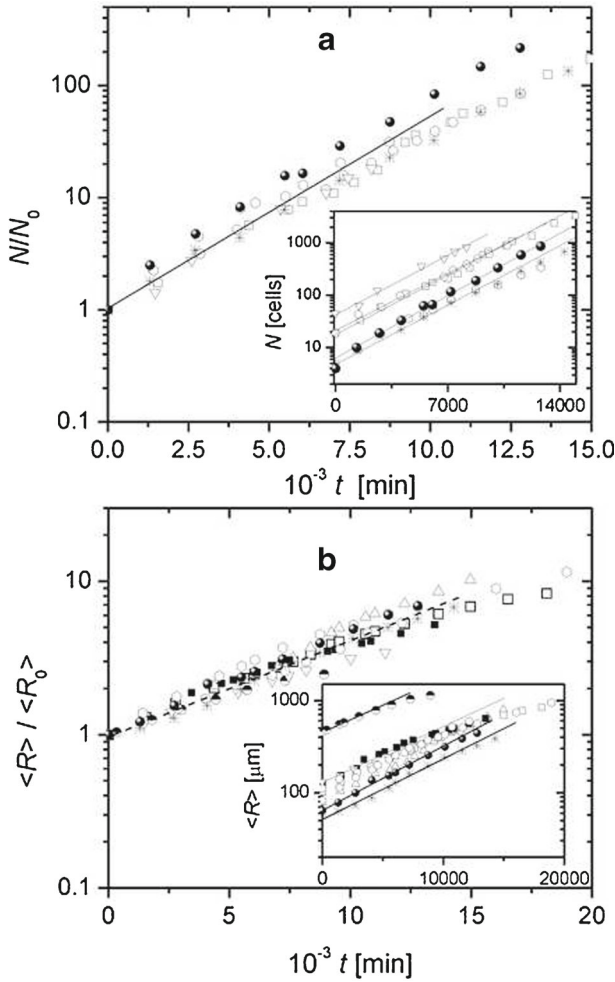
Fig. 2 Log N/N_0 versus t **a** and log $<R>/<R_0>$ versus t **b** plots. Data are taken from QRC patterns. N_0 and $<R_0>$ refer to the number of cells and the average colony radius at $t = 0$, respectively. Insets in **a** and **b** show log N and log $<R>$ versus t plots, respectively. The larger N_0 is, the greater the departure of the experimental data from the straight-line plots becomes

domains, mainly at the border region and 3D cell domains consisting in smaller, quasi-alike, rather compressed groups of cells in the colony bulk were formed. Several events at both the individual cell and the colony scales led to the appearance of spatio-temporal heterogeneities (Fig. 4). In the former case, among these events local cell proliferation and death and the formation of large multinucleated cells generated either by cell fusion [39] or nucleus duplication without cytokinesis [40] were involved. The latter, however, involved the formation of chain-like domains of elongated cells temporarily moving as unstable clusters with preferred directionalities for a certain time [41], the detachment of a small number of cells from the colony either temporarily or definitively and colony 3D spreading. All these events influenced the motility characteristics of individual cells and the spreading kinetic regime transition as described further on.
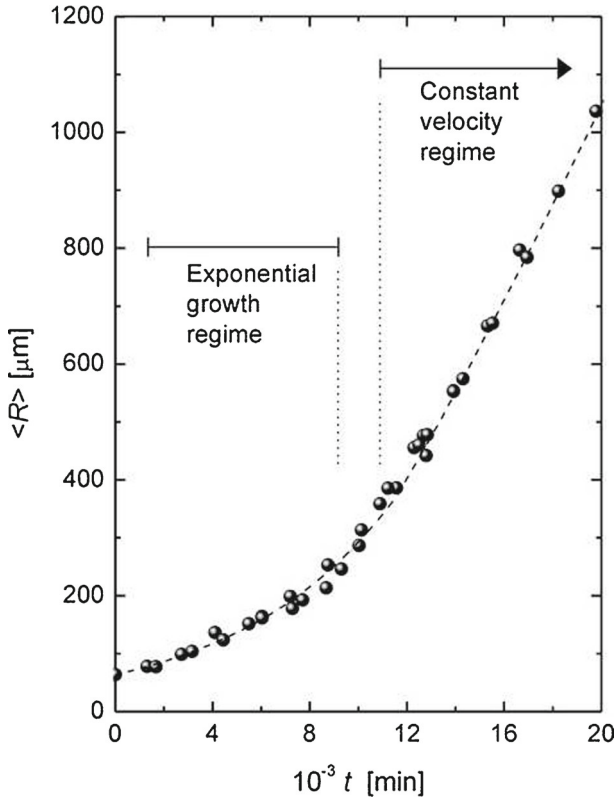
Fig. 3 Plot of $<R>$ versus t from QRC spreading starting from several $<R_0>$ and N_0 at t_0, showing the two kinetic regimes. The dashed trace corresponds to equations (9) and (10) given in reference [25] as described in the text. The exponential to constant $<V_f>$ kinetic transition occurs for about 1500 cells within the 9000 $\leq t \leq 11000$ min range

3.3 Cell density evolution

The cell morphology changes described above induced the formation of spatio-temporal 2D cell domains with different cell densities, i.e., the number of cells per unit area (ρ) that depended on both N and the colony growth geometry. For QRC with $N_0 < 100$ cells, ρ increased from the colony border inwards and its gradient diminished for decreasing $<R>$ and decreasing t (Fig. 5a). Otherwise, for QRC with $N > 1500$ cells (Fig. 5b–c), the density gradient remained almost constant within the range 200–500 μm measured from the colony border inwards, irrespective of t.

For QLC at lower t, the cell density profiles over a 2000 μm colony front length (Fig. 5d) fluctuated around a constant value, approaching a density gradient close to that found for QRC with $N > 1500$ cells. At the initial stage of these runs, after about 24 h from the tape removal, a stationary density profile was obtained. Constraints imposed by the growth geometry at shorter t became evident from the histograms (Fig. 5d). For QRC with $500 \leq N \leq 1500$ cells, the density gradients at 350 μm from the colony border (Fig. 5b) resulted in $(9 \pm 1) \times 10^{-6}$ cells μm^{-3}, a figure greater than $(2 \pm 1) \times 10^{-6}$ cells μm^{-3} for QRC with $N > 1500$ and $(4 \pm 1) \times 10^{-6}$ cells μm^{-3} for QLC.
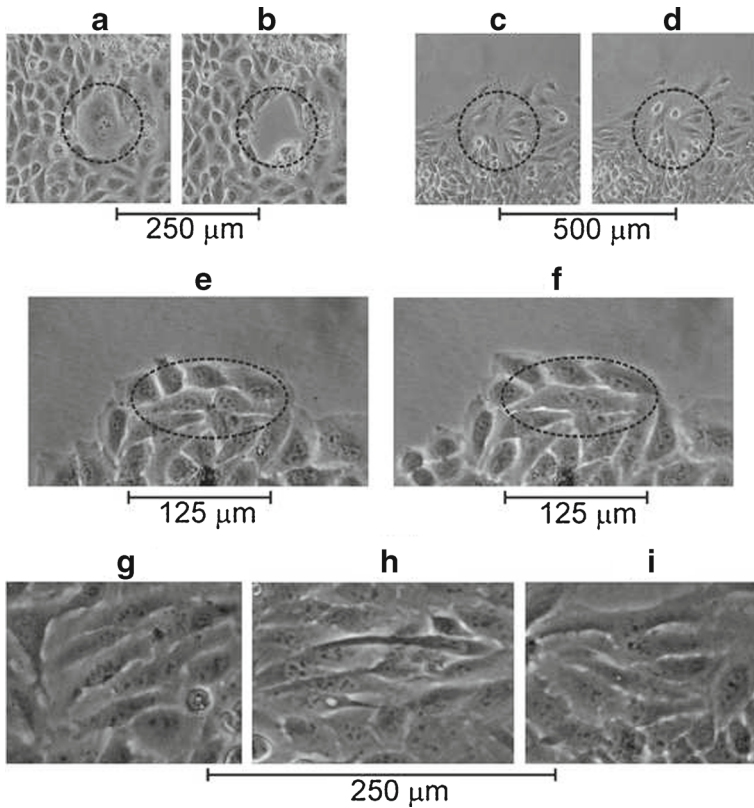
Fig. 4 Colony domains with distinct instantaneous morphologies produced by different events: **a** and **b** death of a large cell and simultaneous cell-free space formation, respectively; **c** and **d** cell duplications; **e** and **f** cell fusion; **g**, **h** and **i** colony domains with almost the same cell shapes displaying quasi-ordered structures

3.4 Individual cell motility

3.4.1 Trajectory and velocity data

Individual cell motilities from QLC and QRC were evaluated by cell tracking at $\Delta t' = 30$ min starting from different N_0, i.e., under both kinetic regimes (Fig. 6). For large N, those cells located at the outermost colony layer followed trajectories longer than those of cells at QRC with low N (Fig. 6b and d). In this case, both 'parent' and 'daughter' cells (Fig. 6e and f) resulting from 85 proliferation events displayed similar tortuous trajectories with a net cell motion component perpendicular to the growth front. Many of these trajectories also displayed significant lateral components persisting for about 300 min over nearly 150 μm.

For QRC and QLC, the analysis of individual cell trajectories at the colony border became useful for interpreting dynamic characteristics at small colony front lengths and looking for local collective cell displacement contributions to the development of colony front protrusions. Thus, cell trajectories from a border region of a QRC with a large N were followed up over 30 h (Fig. 7). Over the first 11 h many cell trajectories contributed
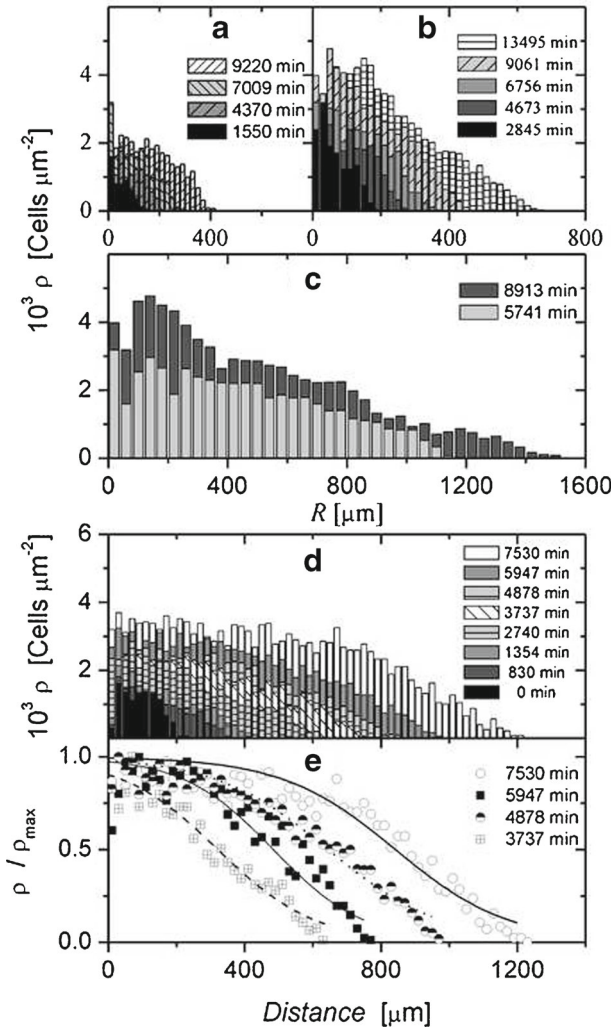
Fig. 5 Cell density profiles from the bulk to the colony border. **a** QRC ($<R_0> = 100\ \mu$m) under exponential kinetic regime; **b** QRC ($<R_0> = 122\ \mu$m) under exponential kinetic regime ($t < 9000$ min) and under constant $<V_f>$ ($t > 9000$ min); **c** QRC ($<R_0> = 430$ m) under constant $<V_f>$; **d** QLC; **e** QLC data fitted with equation (42) from reference [23]. Insets indicate the colony age

to the development of the protrusion (Fig. 7a–c, g), whereas over the following 19 h the protrusion width increased (Fig. 7d–f), involving either existing cells or newborn ones having a remarkable biased trajectory (Fig. 7h). Likewise, a few cells occasionally displayed backward trajectories with low persistence.

For QLC, individual cell average velocities were determined from those cells located in two selected rectangular colony regions (Fig. 8a): region I ($290 \times 450\ \mu$m^2) and region II ($290 \times 600\ \mu$m^2) of comparatively higher and lower ρ. This evaluation was extended up to 12 h, an interval in which the cell density gradient remained almost constant. Each
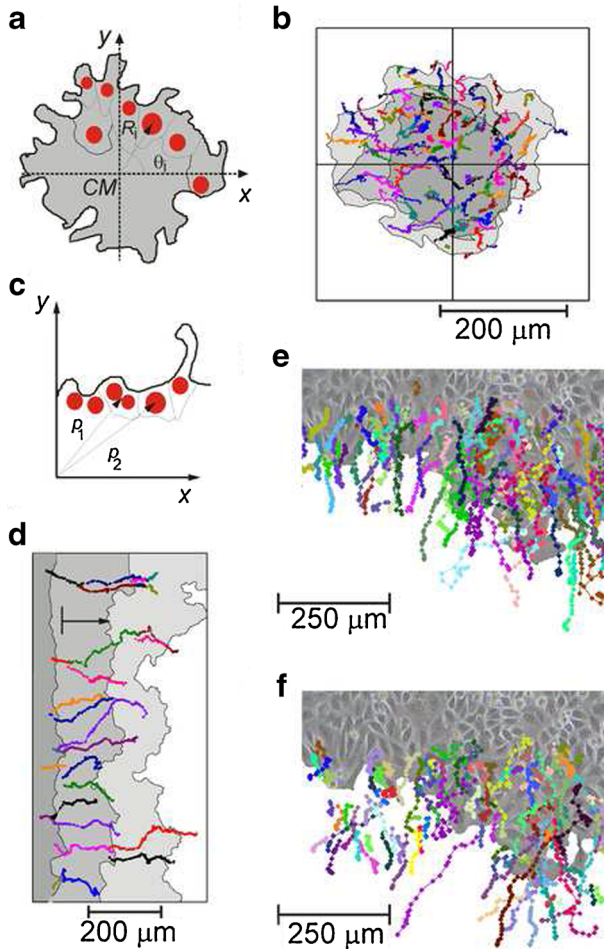
Fig. 6 Basic schemes utilised for determining cell nucleus (red circle) locations at QRC **a** and QLC **c** fronts. Individual cell trajectories from QRC **b** and QLC **d** are identified with different colours. 'Daughter' cell trajectories are also included. Cell trajectory tracking for $\Delta t' = 30$ min was followed over either 62 h **b** or 66 h **d**. Colony fronts at 18 h intervals are identified by the grey colour scale. Initial images of a QLC front and trajectories of selected cells **e** and 'daughter' cells **f** followed over 27 h. Cells exhibit biased trajectories towards the front

region I and II was divided into smaller, contiguous $75 \times 290\ \mu\text{m}^2$ areas to evaluate $<V_{\text{per}}>$ and ρ there. The value of $<V_{\text{per}}>$ versus the distance from the colony border to the centre of regions I (Fig. 8c) and II (Fig. 8d) showed that most cell velocities tended to diminish from the colony border inwards and exhibited some random fluctuations. For about 200 and 500 μm from the colony border, respectively, a correlation of the magnitude of $<V_{\text{per}}>$ fluctuations with the local change of ρ was obtained (Fig. 8b).

Histograms of V_{par} and V_{per} data evaluated for $\Delta t' = 30$ min, for both QRC with different N_0 and QLC, are displayed as semi-logarithmic plots (Fig. 9). The comparison of these plots to Gaussian distributions, indicated by dotted lines in Fig. 9, clearly show a deviation of experimental data at the tails of each distribution, irrespective of the kinetic regime. For
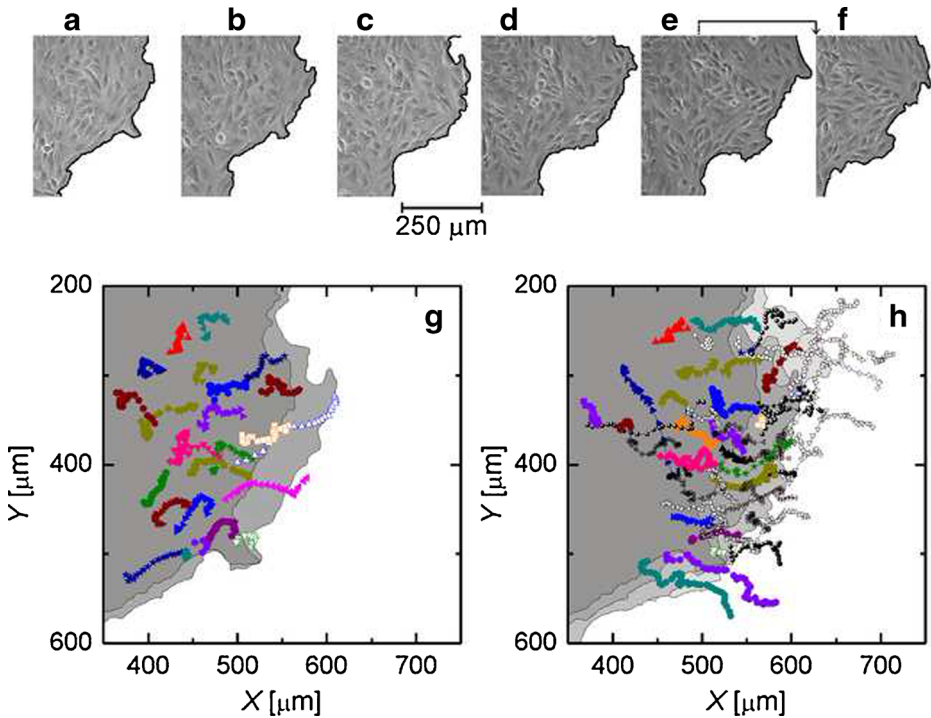
Fig. 7 **a-f** Sequential images taken at 360 min intervals of a QRC ($N > 1500$ cells, $<R_0> = 590$ μm) local front region. Protrusion formation and its subsequent widening can be observed. **g-h** Cell trajectories from colony patterns shown in **a-e** at 30 min intervals. **g** Protrusion formation: cell trajectories from colony patterns depicted in images **a–c** followed over 11 h. **h** Protrusion widening: cell trajectories from colony patterns depicted in images **c–f** followed over 19 h. The grey colour decreasing scale in **g** and **h** indicates the colony border location at $t = 0$, 360 and 1080 min, respectively. Open black symbols indicate new cell trajectories. Net lateral displacements of cells involved in the protrusion widening can be seen

V_{par}, the histogram maxima, despite some fluctuations, remained close to zero. In contrast, for V_{per}, the histogram maxima exhibited a positive shift as N increased with the tendency to approach a constant V_{per}. For both V_{par} and V_{per} in going from QRC under exponential kinetic regime to QLC and QRC under constant $<V_f>$, the dispersion of data increased, although for QRC, in this case, the dispersion was larger than for QLC.

The evolution of each cell trajectory for $\Delta t' = 30$ min depended on its instantaneous directionality (D/T) defined as the ratio between the shortest linear distance between the initial and final cell position (D) and the total cell trajectory (T). In these cases $\Delta t'$ was sufficiently large to minimise the influence of cell membrane fluctuations on cell trajectories. Accordingly, D/T values should be within the range $0 \leq D/T \leq 1$, i.e., the limiting figures that would be expected for either a random-like or ballistic-like trajectory, respectively.

D/T histograms (Fig. 10) depended on both the colony spreading kinetic regime and the colony geometry. D/T histogram maxima shifted from 0.8 for QLC at constant $<V_f>$ to about 0.2 for QRC under exponential kinetic regime. These results confirm that biased contributions to cell trajectories decreased in going from (a) to (d). They became most remarkable from QLC data.
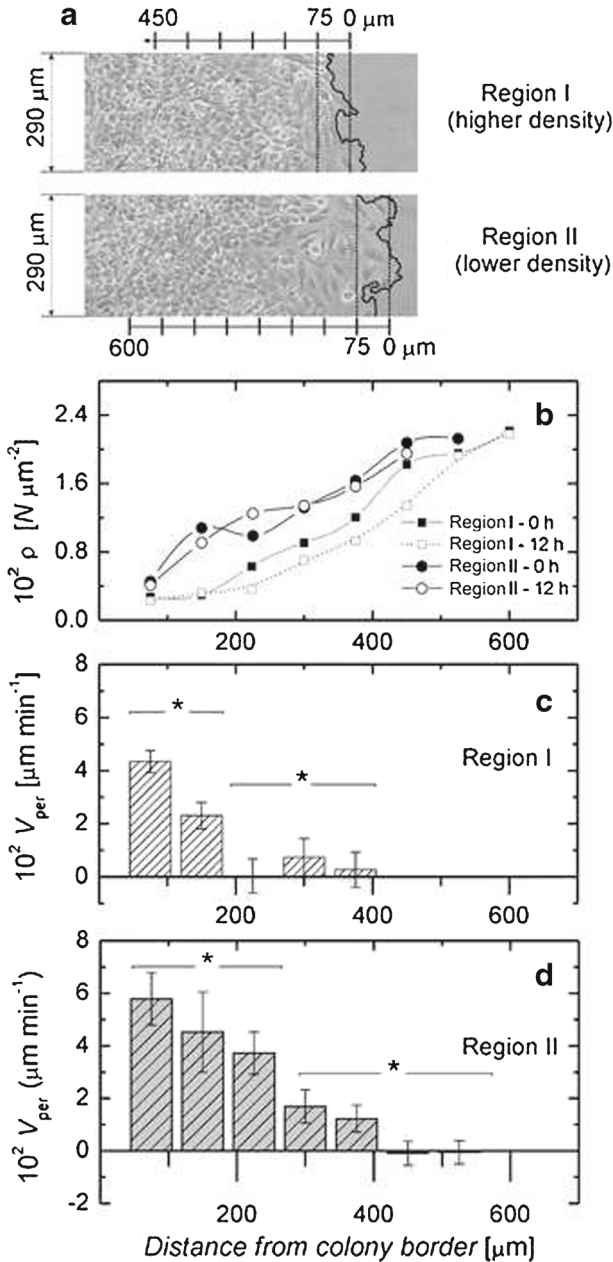
Fig. 8 **a** Regions I (higher cell density) and II (lower cell density) of a QLC. Scales were drawn to identify the colony areas where individual cell velocity data were obtained. The origins of length scales are taken at the respective average front locations (dashed trace). **b** Local cell density versus the distance from the colony front depicted in **a** at $t = 0$ h and $t = 12$ h for regions I and II, as indicated. **c** and **d** Values of $<V_{per}>$ resulting from cells located in different areas of regions I and II versus their distance from the colony border. Standard errors are included. The ANOVA test (0.01 significance level) was used to probe differences in $<V_{per}>$ resulting from the areas of regions I and II as indicated by the stars
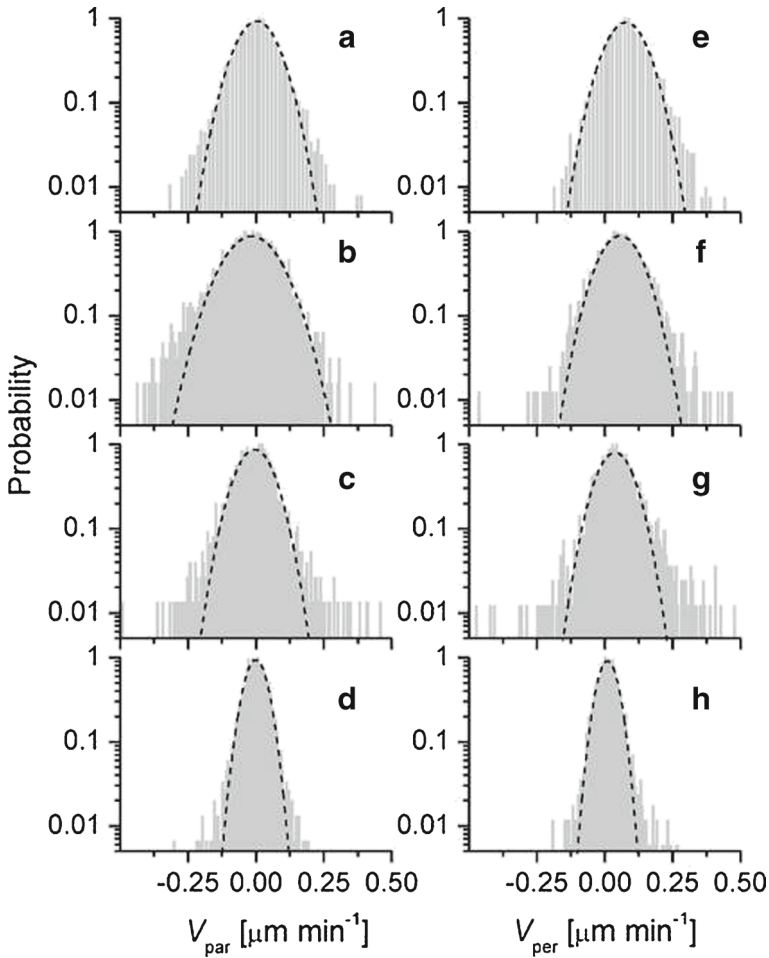
Fig. 9 Semi-logarithmic plots of V_{par} histograms **a–d** and of V_{per} histograms **e–h**. **a** and **e**: QLC data under constant $<V_f>$; **b** and **f**: QRC ($<R_0> = 590\ \mu$m) under constant $<V_f>$; **c**, **d** and **g**, **h**: QRC under exponential kinetic regime ($<R_0> = 200\ \mu$m) **c** and **g** and for $<R_0> = 108\ \mu$m **d** and **h**. Each histogram includes data from triplicate runs at least, considering 4000–5500 data items for each histogram. The Gaussian distribution functions are displayed to show the non-Gaussian behaviour of the experimental data. The ANOVA test (0.01 significance level) was used to probe significant differences in the maximum of V_{per}. Differences for V_{par} approach zero

3.4.2 Individual cell mean square displacements

Despite their dispersion, individual cell msd versus Δt log-log plots from both QRC (msd_{QRC}) under exponential kinetic regime (Fig. 11a) and QLC (msd_{QLC}) (Fig. 11b) showed that msd_{QLC} became about one order of magnitude greater than msd_{QRC}. Thus, a number of plots of individual cells closely fulfilled a straight line with either 1 or 2 slope. About one half of the msd_{QRC} plots within the 1000–3000 min range (Fig. 11a) were bent towards the straight line with slope 2, whereas for msd_{QLC} data the same situation was observed within the 700–2000 min range (Fig. 11b). Some plots occasionally exhibited short

Fig. 10 Histograms of individual cell directionalities (D/T); **a** QLC and **b** QRC ($<R_0>= 590\,\mu$m), both under constant $<V_f>$; **c** QRC ($<R_0>= 200\,\mu$m) data under exponential kinetic regime; **d** the same as in **c** for $<R_0>= 108\,\mu$m. The evolution of each cell trajectory at $\Delta t' = 30$ min depended on its instantaneous directionality (D/T)
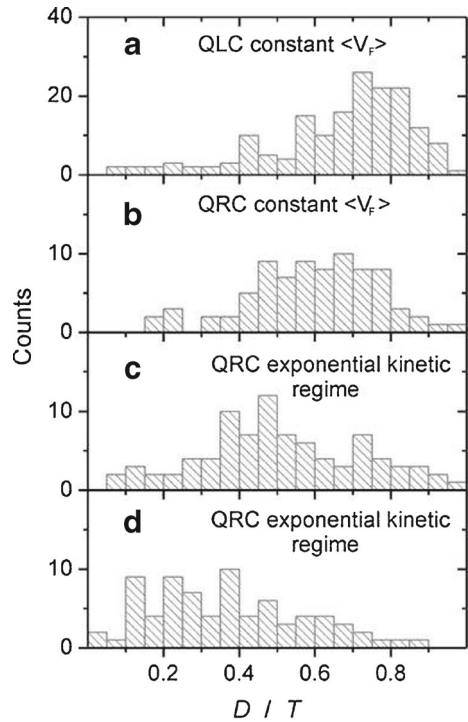
straight line portions with a negative slope, a fact that was consistent with cell trajectory features described in Section 3.4.1. It should be noted that the greater the error in *msd* data was, the longer Δt became. Then, fluctuations in those plots can be due, at least in part, to the local colony morphology changes described above (Fig. 4). The above description is consistent with the influence of colony heterogeneity on individual cell motility.

Likewise, at intermediate Δt, average experimental data (open circles in Fig. 10) fitted straight line dependences with different slopes between 1 and 2 within certain ranges of Δt. Thus, for QRC under exponential kinetic regime, the average slope resulted in 1.4±0.1 over the range $120 \leq \Delta t \leq 750$ min (Fig. 11b), whereas for QLC under constant $<V_f>$ it was 1.7±0.1 over the range $90 \leq \Delta t \leq 700$ min (Fig. 11b). These Δt ranges depended on both N and the colony geometry. Furthermore, average data from both QRC and QLC tended to approach two asymptotic straight lines, one with slope 1 at the shortest Δt and the other with slope 2 at the longest Δt. Cell motility at QRC, for $\Delta t < 400$ min or thereabouts, involved a large number of cell displacements with slope 1 in the *msd* versus Δt plots, whereas the reverse situation was found for QLC.

The contribution of each aforementioned asymptotic behaviour to individual cell displacements is shown in Fig. 12, where the difference between average *msd* data for either QLC or QRC and the *msd* resulting from the asymptotic random walk (*arw*) curve versus Δt (msd_{arw}) (curves Φ and Ω, respectively) is plotted for $90 \leq \Delta t \leq 900$ min. The *arw* curve was obtained from QRC data under exponential kinetic regime ($\Delta t \rightarrow 0$). The relative increase in curves Φ and Ω with Δt suggested that the contribution of ballistic-type motility for QLC became greater than for QRC under exponential kinetic regime. The comparison of curves Ω and Φ pointed out that cell migration involved a collective contribution from neighbour cells.
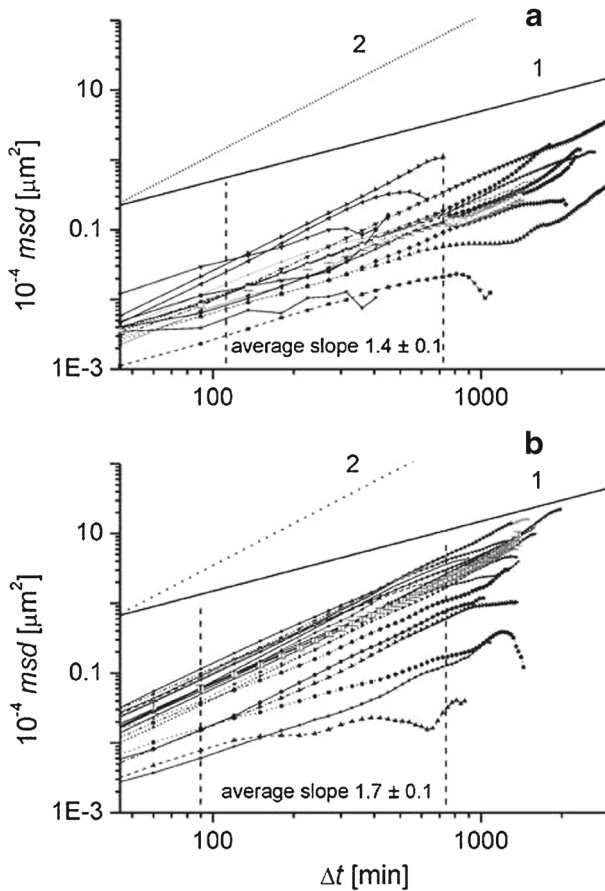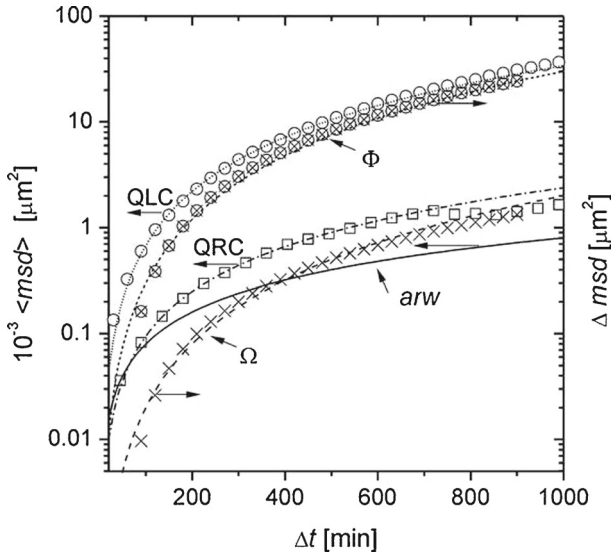
Fig. 11 Log *msd* versus log Δt plots. **a** Data from the smallest QRC shown in Fig 6a. **b** Data from QLC. Average *msd* data from tracked cells within the range 30–1800 min are plotted (larger open symbols) and standard error bars are indicated. Straight lines with the limiting slopes 1 and 2 are included for guidance. The average slopes of the best straight line fittings for QRC **a** and QLC **b** and their corresponding Δt ranges are indicated

3.5 Influence of neighbour cells

The correlation between the individual cell average velocity and the local cell density (Fig. 8) demonstrated that cell motility is influenced by neighbour cells, regardless of the colony 2D growth kinetic regime. This dependence can be analysed utilising a rather simple landscape. Let us consider a 130 μm diameter circular colony domain with a central reference cell surrounded by a certain number of neighbour cells. The reference cell is located either at the colony front (case I) (Fig. 13) or in 2D colony bulk domains (case II) (Fig. 14). Neighbour cell nucleus coordinates were followed as long as cells remained inside the circle. For both case I and II the reference cell trajectory directions (arrows) (Figs. 13–14) were pointing out from a higher to a lower number of cell density domains.

For case I, the initial portion of the reference cell trajectory included most neighbour cells on the up right side of the circular region (Fig. 13a). Subsequently, the reference cell moved

Fig. 12 Log $<msd>$ versus Δt plots and log Δmsd, i.e., the average difference between experimental msd data and those resulting from the asymptotic random walk (arw) (full trace) versus Δt plots. Data from Fig. 11 for $90 < \Delta t < 900$ min were utilised. (O) Experimental QLC data (msd_{QLC}); ($\square$) experimental QRC data (msd_{QRC}); ($\otimes$) $msd_{QLC} - msd_{arw}$ versus Δt (curve Φ); (x) $msd_{QRC} - msd_{arw}$ versus Δt (curve Ω)
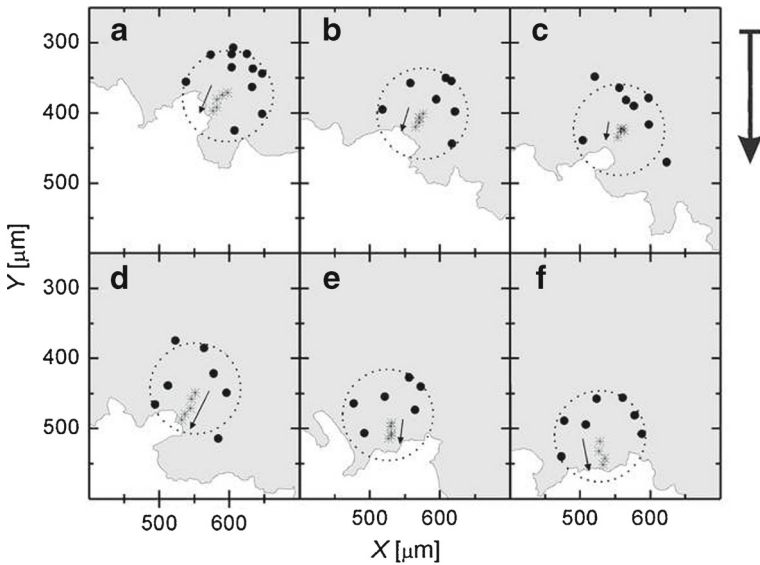
Fig. 13 Motility of a reference cell (*star*) initially located at the centre of a 130 μm diameter 2D circular region including the colony border (*dashed circle*) (case I) and neighbour cells in it (*black dots*). Arrows in each figure indicate the nucleus coordinate motion direction of the reference cell in the *X-Y* plane. These coordinates are evaluated at $\Delta t = 30$ min over 150 min. Coordinates of neighbour cell nuclei are plotted at $\Delta t = 150$ min **a–f**. The reference cell motion direction exhibits a bias caused by neighbour cells. The outer arrow indicates the main colony front motion direction. Shaded regions correspond to colony domains
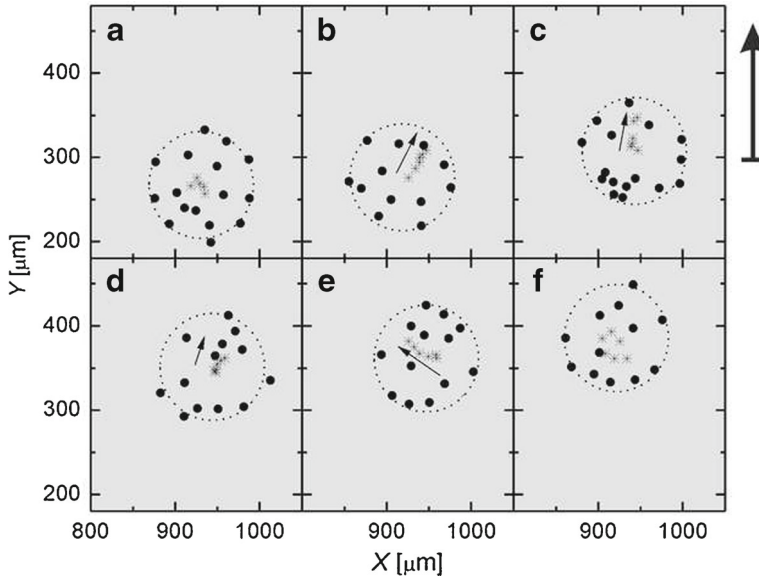
Fig. 14 Motility of a reference cell (*star*) initially located at the centre of a 130 μm diameter 2D circle in the colony bulk region (*dashed circle*) surrounded by a number of neighbour cells (*black dots*) (case II). Symbol references and measurement conditions are the same as those indicated in Fig. 13. The reference cell motion direction feels the influence of a bias caused by the environment. The outer arrow indicates the main colony front motion direction

in a left tilted downward direction (Fig. 13b and c). Further colony expansion showed that the reference cell shifted in a slightly right tilted downward direction and the number of neighbour cells diminished (Fig. 13f).

For case II, the density of neighbour cells was significantly higher than for case I (Fig. 14). At the beginning, the reference cell fluctuated around its original location but as the neighbour cell density increased on the low left side of the circular domain, the reference cell moved upwards to the right. Later, its direction changed to the left as the density of the neighbour cells on the up right side increased. Occasionally, the reference cell remained almost at rest for about 150 min, although suffering deformations. This situation was scarcely probable for case I because the distribution of the neighbour cells in the circular region became more asymmetric than for case II.

4 Discussion

4.1 A survey of kinetic and morphology aspects of HeLa cell colonies

The N-dependent 2D spreading kinetic transition from exponential law to the constant $<V_f>$ regime (Section 3.1) has earlier been reported for distinct cell lines [42–46] and interpreted through different 2D cell colony spreading mechanisms [42, 47–50]. On the other hand, colony morphology patterns (Section 3.2.) showed that those regimes were related to the degree of spatio-temporal heterogeneities built up in the colony by changes in cell shape,

size, cell-cell average distance, i.e., local cell density, cell proliferation decreasing inward [51–53] and formation of 3D domains at the colony bulk. Cell proliferation in these domains contributed to increasing the 3D phase but had a minor influence on 2D spreading. All these changes depended on N and became, to a great extent, responsible for the colony kinetic transition referred to above. For both QRC and QLC at constant $<V_f>$, due to cell proliferations localised within an outer effective 2D region of an almost constant average thickness from the colony border inwards, a constant cell density gradient built up there (Fig. 5c–d).

On the other hand, QRC involved the simultaneous increase of both the colony mass and space, whereas QLC entailed the increase of the colony mass maintaining the front width constant. Thus, the colony geometry influence on the spreading kinetic regime became evident from both cell densities and their gradients, which for QRC (Fig. 5c) was lower than for QLC (Fig. 5d). The similarity of $<V_f>$ values resulting from both colony geometries was consistent with the larger average size of cells at the QRC border region than at the QLC one (Fig. 5c).

The model that has been proposed in reference [25] for an increasing colony radius was utilised to interpret our QRC spreading kinetic data (Fig. 3). Considering average cell diameter $<a> = 25 \mu m$, and $<\tau> = 2400$ min for the biosystem with $N < 1000$ cells from Section 3.1, the effective border region thickness resulted in $\Delta L_{eff} = 210 \mu m$. Furthermore, data depicted in Fig. 5e were fitted with equation (42) from reference [23] allowing the evaluation of $<k_0>$, the duplication constant of a cell at the uncrowded environment and D_o, the diffusion constant of an isolated cell. From data fitting, it followed that $<k_0> = 4 \pm 1 \times 10^{-4}$ min^{-1}, in agreement with the kinetic constant from data reported in Section 3.1 and $D_o = 9 \pm 2 \mu m^2$ min^1. This figure was within the order range of D_o, which was obtained from 3T3 fibroblast during the development of a confluent cell monolayer ($D_o = 3 \mu m^2$ min^1) and in a wound healing assay ($D_o = 5.5 \mu m^2$ min^1), although the larger value of the latter is consistent with the asymmetry imposed on cell migration due to the experimental arrangement. A similar value ($D_o = 11.4 \mu m^2$ min^1) has been reported for isolated glioma cells migrating in the direction of decreasing the gradient of a chemorepellent agent [54]. Therefore, the multi-scale model formalism appears to be coherent with the spatio-temporal heterogeneities in the colony, their influence on the cell migration process, throughout cell density-dependent inhibition effects.

Nevertheless, despite the above reasonable agreement of our experimental data with the prediction of the models (Figs. 3 and 5e), it should be noted that the complex influence of spatio-temporal heterogeneities on the dynamics of the biosystem in a standard medium (Figs. 1, 3 and 4) still remains rather vague.

4.2 Dynamic aspects of individual cells

For QRC ($N < 1000$) the value of $<V_{per}>$, the average celerity and the D/T ratio increased with N (Figs. 9 and 10), approaching the behaviour of QLC. For both QRC ($N > 1500$ cells) and QLC border regions, the average velocity of individual cells diminished from the colony border inwards. For QLC, the value of $<V_{per}>$ decreased to about one-half at 200–300 μm from the colony edge inwards, i.e., a length comparable to that utilised in Section 4.1 for ΔL_{eff}. Likewise, individual cell velocities at the 2D border region exhibited a reverse dependence on the average cell-cell distance (Fig. 8). A similar behaviour has been reported for other condensed phase front velocity displacements, irrespective of their inorganic [55] or biological nature [56]. The above description is consistent with local crowding [57–59] effects that increased with N. Correspondingly, as both the colony radius and the

spatio-temporal heterogeneity of cell domains in the colony increased, local crowding had a more remarkable bias contribution to individual cell trajectories, particularly at the border region (Figs. 13 and 14). Therefore, the crowding effect on individual cell motility is a complex phenomenon in which the organisation of the colony and the shape and orientation fluctuations of each group of cells as agents play a key role in the collective migration of cells.

The *msd* dependence on Δt (Fig. 11) was consistent with the contribution of N-dependent cooperative effects from neighbour cells in the collective cell transport described in Section 3.4.2. Accordingly, the random walk-like mechanism ($b = 1$) became dominant for QRC at low N and low Δt, i.e., when the colony growth geometry provided more free space for allocating new and already existing cells, whereas the ballistic-like mechanism ($b = 2$) became relevant at both QRC with large N and QLC at long Δt.

Recently, the monolayer stress microscopic technique was introduced to obtain the local state of stress within a cell sheet of colonies with large N. From the 2D balance of cell-substrate traction forces, after applying Newton's law, the distribution of line forces everywhere within the cell sheet was obtained [32, 33]. Stresses have been related to the accumulation of traction forces applied on the underside of the cells, which results in spontaneous severe mechanical stress fluctuations within the cell sheet and ripples across it. Correspondingly, these fluctuations exhibit a broad non-Gaussian distribution, become increasingly rugged, sluggish and cooperative as the cell density increases. Accordingly, the collective effect of neighbour cells on individual cell motility involves joint forces for enhancing normal stresses across cell-cell junctions, assisting in cell migration in directions of diminishing intercellular shear stress. It has also been suggested that 'leader' cells play a pivotal role in local cell guidance as the main physical forces they generate are just a part of the global tug-of-war involving cells well back from the leading edge. Migration of both epithelial and endothelial cells in colonies as well as cancer cell lines before the epithelial-mesenchymal transition can reasonably be explained by the above description. This explanation is qualitatively consistent with the cell trajectory characteristics described in Section 3.

However, the difference in the average individual cell motility as well as in the cell density profiles (Fig. 5) observed when N increased from 100 to 1500 cells could be associated with a change in the balance of forces according to the above-described framework, which should imply a positive relationship between the cell density and the local mechanical stress [32, 33].

4.3 Front roughness scaling and individual cell trajectories

Roughness fluctuation data of 2D QRC ($N > 1500$ cells) and QLC fronts were derived from the dynamic scaling theory and Fourier data analysis [29, 33, 60, 61]. Following these approaches it was found that the 2D front roughness dynamics fulfilled the set of roughness exponents $\alpha = 0.50 \pm 0.05$, $\beta = 0.32 \pm 0.04$ and $z = 1.5 \pm 0.2$, within the experimental ranges $0 < t < 10^4$ min and $10^2 < l < 10^3 \mu$m, irrespective of the growth geometry [29]. This set of exponents agreed with that predicted by the KPZ 1D universality class [27, 30]. Accordingly, the standard KPZ front velocity displacement equation involves three terms. (i) A smoothing Laplacian term that represents any diffusion process with constant diffusivity or processes involving a constant surface tension, diminishing the curvature of the protrusion and decreasing its height. This term is associated with the random-like cell motility contribution. (ii) A non-linear term with a coefficient λ that accounts for the contribution of biased cell trajectories resulting from spatio-temporal heterogeneities (anisotropies)

originated in the system to the behaviour of individual cells searching for free space at the colony front region. Cell biased displacements greatly determine the formation and widening of protrusions as described in the previous sections. This process should mainly be associated with the ballistic-like cell motility contribution. (iii) A stochastic term that should principally involve the cell proliferation dynamics at the 2D cell layer. Improved versions of the KPZ 1D and 2D equations have recently been proposed [62, 63], including the KPZ formality to 2D cell colony spreading on a tessellation-structured lattice [31]. The analysis of the internal structure of the system under propagation as well as distinct lattice scale events were also considered to infer the universality of the processes as an alternative to the roughness dynamic scaling analysis [64–66].

Recently reported experimental evidence about the dependence of the universal statistical properties on the global geometry of the interface [67–69] provided the possibility of looking for some qualitative relationships between cell motility characteristics and the KPZ roughness dynamics. In our work, the influence of the directionality of cell trajectories on the KPZ behaviour depended on the average radius of curvature of the colony interface. On the other hand, the local V_{per}/V_{par} ratio should be influenced by the cell aspect ratio of one or a group of cells. An influence of this type has been reported in reference [26]. For large$<R>$ there is a tendency of QRC to approach the behaviour of QLC. Correspondingly, both geometries exhibit an asymmetry in the interface fluctuations involving a positive coefficient $\lambda > 0$ affecting the non-linear terms in the KPZ equation that reveals the cell biased trajectory characteristics. This fact is consistent with the asymmetry of interface fluctuations reported in reference [69] for linear geometry.

5 Conclusions

1. The 2D spreading of HeLa cell colonies exhibited two N-dependent growth regimes, an exponential one for QRC with $N < 1000$ cells and a constant average front velocity regime for QLC and QRC with $N > 1500$ cells.
2. The above kinetic transition was largely related to the development of spatio-temporal heterogeneities in the colony. At constant average front velocity, the colony was described as a 2D effective border region with a constant average thickness and a bulk region with 3D phase formation. Cell proliferation and migration within the 2D effective region largely contributed to the colony front displacement. Individual cell motility in this region was cooperatively increased by the presence of neighbour cells due to local crowding effects. In contrast, in the bulk region, an inhibition of cell motility due to crowding effects set in. Cell proliferation there was also largely inhibited.
3. Either the radial or linear growth geometry specifically influenced the cell size and shape and the distribution of both cell density and spatio-temporal heterogeneities in the colony. The average front constant velocity displacement was almost the same for both QLC and QRC despite their different free space dilation. This fact was partially due to a compensation of the cell average size that was larger at the QRC border region than at the QLC one and the greater free space created by QRC expansion for cell allocation.
4. Dynamic data suggested that cell motility fulfilled a concerted mechanism involving the contribution of a random walk-like and a ballistic-like process. Their ratio became smaller as N increased.
5. Individual cell biased trajectories had cell parallel and perpendicular velocity components with respect to the colony front. The ratio of these components had a remarkable

influence on the cell directionality. The random-to-ballistic contribution ratio in cell motility had a remarkable effect on the 2D colony roughness and the protrusion width evolution features.

6. Experimental data for both QLC and QRC are consistent with the fulfilment of the KPZ-like equation with $\lambda > 0$ for 2D HeLa cell colony front roughness and protrusion formation, at least within certain ranges of colony front length and time.

References

1. Gurtner, G.C., Werner, S., Barrandon, Y., Longaker, M.T.: Wound repair and regeneration. Nature **453**, 314–321 (2008)
2. Lecaudey, V., Gilmour, D.: Organizing moving groups during morphogenesis. Curr. Opin. Cell Biol. **18**, 102–107 (2006)
3. Chicoine, M.R., Silbergeld, D.L.: The in vitro motility of human gliomas increases with increasing grade of malignancy. Cancer **75**, 2904–2909 (1995)
4. Kumar, S., Weaver, M.V.: Mechanics, malignancy, and metastasis: The force journey of a tumor cell. Cancer Metast. Rev. **28**, 113–127 (2009)
5. Yamazaki, D., Kurisu, S., Takenawa, T.: Regulation of cancer cell motility through actin reorganization. Cancer Sci. **96**, 379–386 (2005)
6. Li, S., Guan, J.-L., Chien, S.: Biochemistry and biomechanics of cell motility. Annu. Rev. Biomed. Eng. **7**, 105–150 (2005)
7. Fletcher, D.A., Theriot, J.A.: An introduction to cell motility for the physical scientist. Phys. Biol. **1**, T1–T10 (2004)
8. Selmeczi, D., Mosler, S., Hagedorn, P.H., Larsen, N.B., Flyvbjerg, H.: Cell motility as persistent random motion: theories from experiments. Biophys. J. **89**, 912–931 (2005)
9. Douezan, S., Dumond, J., Brochard-Wyart, F.: Wetting transitions of cellular aggregates induced by substrate rigidity. Soft Matt. **8**, 4578–4583 (2012)
10. DiMilla, P.A., Stone, J.A., Quinn, J.A., Albelda, S.M., Lauffenburger, D.A.: Maximal migration of human smooth muscle cells on fibronectin and type IV collagen occurs at an intermediate attachment strength. J. Cell Biol. **122**, 729–737 (1993)
11. Montell, D.J.: Morphogenetic cell movements: diversity from modular mechanical properties. Science **322**, 1502–1505 (2008)
12. Alt-Holland, A., Zhang, W., Margulis, A., Garlick, J.A.: Microenvironmental control of premalignant disease: the role of intercellular adhesion in the progression of squamous cell carcinoma. Semin. Cancer Biol. **15**, 84–96 (2005)
13. Tzvetkova-Chevolleau, T., Stéphanou, A., Fuard, D., Ohayon, J., Schiavone, P., Tracqui, P.: The motility of normal and cancer cells in response to the combined influence of the substrate rigidity and anisotropic microstructure. Biomaterials **29**, 1541–1551 (2008)
14. Friedl, P., Glimour, D.: Collective cell migration in morphogenesis, regeneration and cancer. Nat. Rev. Mol. Cell Biol. **10**, 445–457 (2009)
15. Yin, J., Xu, K., Zhang, J., Kumar, A., Yu, F.-S.X.: Wound-induced ATP release and EGF receptor activation in epithelial cells. J. Cell Sci. **120**, 815–825 (2007)
16. Nicklić, D.L., Boettiger, A.N., Bar-Sagi, D., Carbeck, J.D., Shvartsman, S.Y.: Role of boundary conditions in an experimental model of epithelial wound healing. Am. J. Physiol. Cell Physiol. **291**, C68–C78 (2006)
17. Poujade, M., Grasland-Mongrain, E., Hertzog, A., Jouanneau, J., Chavrier, P., Ladoux, B., Buguin, A., Silberzan, P.: Collective migration of an epithelial monolayer in response to a model wound. Proc. Natl. Acad. Sci. USA **104**, 15988–15993 (2007)
18. Sengers, B.G., Please, C.P., Oreffo, R.O.C.: Experimental Characterization and computational modelling of two-dimensional cell spreading for skeletal regeneration. J. R. Soc. Interface **4**, 1107–1117 (2007)

19. Farooqui, R., Fenteany, G.: Multiple rows of cells behind an epithelial wound edge extend cryptic lamellipodia to collectively drive cell-sheet movement. J. Cell Sci. **118**, 51–63 (2005)
20. Bindschadler, M., McGrath, J.L.: Sheet migration by wounded monolayers as an emergent property of single-cell dynamics. J. Cell Sci. **120**, 876–884 (2006)
21. Takamizawa, K., Niu, S., Matsuda, T.: Mathematical simulation of unidirectional tissue formation: in vitro transanastomotic endothelization model. J. Biomater. Sci. Polym. Ed. **8**, 323–334 (1996)
22. Savla, U., Olson, L.E., Waters, C.M.: Mathematical modeling of airway epithelial wound closure during cyclic mechanical strain. J. Appl. Physiol. **96**, 566–574 (2004)
23. Cai, A.Q., Landman, K.A., Hughes, B.D.: Multi-scale modeling of a wound-healing cell migration assay. J. Theor. Biol. **245**, 576–594 (2007)
24. Lushnikov, P.M., Chen, N., Alber, M.: Macroscopic dynamics of biological cells interacting via chemotaxis and direct contact. Phys. Rev. E **78**, 061904 (2008)
25. Radszuweit, M., Block, M., Hengstler, J.G., Schöll, E., Drasdo, D.: Comparing the growth kinetics of cell populations in two and three dimensions. Phys. Rev. E **79**, 051907 (2009)
26. Simpson, M.J., Baker, R.E., McCue, S.W.: Models of collective cell spreading with variable cell aspect ratio: a motivation for degenerate diffusion models. Phys. Rev. E **83**, 021901 (2011)
27. Barabasi, A.L., Stanley, H.E.: Fractal concepts in surface growth. Cambridge University Press, Cambridge (1993)
28. Meakin, P.: Fractal, Scaling and Growth Far from Equilibrium. Cambridge University Press, Cambridge (1998)
29. Huergo, M.A.C., Pasquale, M.A., Bolzán, A.E., González, P.H., Arvia, A.J.: Growth dynamics of cancer cell colonies and their comparison with noncancerous cells. Phys. Rev. E **85**, 011918 (2012)
30. Kardar, M., Parisi, G., Zhang, Y.-C.: Dynamic scaling of growing interfaces. Phys. Rev. Lett. **56**, 889–892 (1986)
31. Block, M., Schöll, E., Drasdo, D.: Classifying the expansion kinetics and critical surface dynamics of growing cell populations. Phys. Rev. Lett. **99**, 248101 (2007)
32. Trepat, X., Wasserman, M.R., Angelini, T.E., Millet, E., Weitz, D.A., Butler, J.P., Fredberg, J.J.: Physical forces during collective cell migration. Nat. Phys. **5**, 426–430 (2009)
33. Tambe, D.T., Hardin, C.C., Angelini, T.E., Rajendran, K., Park, C.Y., Serra-Picamal, X., Zhou, E.H., Zaman, M.H., Butler, J.P., Weitz, D.A., Fredberg, J.J., Trepat, X.: Collective cell guidance by cooperative intercellular forces. Nat. Mater. **10**, 469–475 (2011)
34. Huergo, M.A.C., Pasquale, M.A., Bolzán, A.E., Arvia, A.J., González, P.H.: Morphology and dynamic scaling analysis of cell colonies with linear growth fronts. Phys. Rev. E **82**, 031903 (2010)
35. Huergo, M.A.C., Pasquale, M.A., Bolzán, A.E., González, P.H., Arvia, A.J.: Dynamics and morphology characteristics of cell colonies with radially spreading growth fronts. Phys. Rev. E **84**, 021917 (2011)
36. Rieu, J.P., Upadhyaya, A., Glazier, J.A., Ouchi, N.B., Sawada, Y.: Diffusion and deformations of single hydra cells in cellular aggregates. Biophys. J. **79**, 1903–1914 (2000)
37. Diambra, L., Cintra, L.C., Chen, Q., Schubert, D., Costa, L., da, F.: Cell adhesion protein decreases cell motion: statistical characterization of locomotion activity. Physica. A **365**, 481–490 (2006)
38. Li, L., Wang, B.H., Wang, S., Moalim-Nour, L., Mohib, K., Lohnes, D., Wang, L.: Individual cell movement, asymmetric colony expansion, rho-associated kinase, and E-cadherin impact the clonogenicity of human embryonic stem cells. Biophys. J. **98**, 2442–2451 (2010)
39. Chen, E.H., Grote, E., Mohler, W., Vignery, A.: Cell-cell fusion. FEBS Lett. **581**, 2181–2193 (2007)
40. Straight, A.F., Cheung, A., Limouze, J., Chen, I., Westwood, N.J., Sellers, J.R., Mitchison, T.J.: Dissecting temporal and spatial control of cytokinesis with a myosin II inhibitor. Science **299**, 1743–1747 (2003)
41. Haga, H., Irahara, C., Kobayashi, R., Nakagaki, T., Kawabata, K.: Collective movement of epithelial cells on a collagen gel substrate. Biophys. J. **88**, 2250–2256 (2005)
42. Freyer, J.P., Sutherland, R.M.: A reduction in the in situ rates of oxygen and glucose consumption of cells in EMT6/Ro spheroids during growth. J. Cell. Physiol. **124**, 516–24 (1985)
43. Mueller-Klieser, W., Freyer, J.P., Sutherland, R.M.: Influence of glucose and oxygen supply conditions on the oxygenation of multicellular spheroids. Br. J. Cancer **53**, 345–353 (1986)
44. Brú, A., Albertos, S., Subiza, J.L., García-Asenjo, J.L., Brú, I.: The universal dynamics of tumor growth. Biophys. J. **85**, 2948–2961 (2003)
45. Galle, J., Hoffmann, M., Aust, G.: From single cells to tissue architecture: a bottom-up approach to modelling the spatio-temporal organisation of complex multi-cellular systems. J. Math. Biol. **58**, 261–283 (2009)
46. Galle, J., Sittig, D., Hanisch, I., Wobus, M., Wandel, E., Loeffler, M., Aust, G.: Individual cell-based models of tumor-environment interactions: multiple effects of CD97 on tumor invasion. Am. J. Pathol. **169**, 1802–1811 (2006)

47. Drasdo, D., Hoehme, S.: A single-cell-based model of tumor growth in vitro: monolayers and spheroids. Phys. Biol. **2**, 133–147 (2005)
48. Menchón, S.A., Condat, C.A.: Cancer growth: Predictions of a realistic model. Phys. Rev. E **78**, 022901 (2008)
49. Galle, J., Loeffler, M., Drasdo, D.: Modeling the effect of deregulated proliferation and apoptosis on the growth dynamics of epithelial cell populations in vitro. Biophys. J. **88**, 62–75 (2005)
50. Drasdo, D., Hoehme, S., Block, M.: On the role of physics in the growth and pattern formation of multi-cellular systems: What can we learn from individual cell-based models. J. Stat. Phys. **128**, 287–345 (2007)
51. Dulbeco, R., Stoker, M.G.: Conditions determining initiation of DNA synthesis in 3T3 cells. Proc. Natl. Acad. Sci. USA **66**, 204–210 (1970)
52. Todaro, G.J., Lazar, K.G., Green, H.: The initiation of cell division in a contact-inhibited mammalian cell line. J. Cell. Physiol. **66**, 325–333 (1965)
53. Turner, S., Sherratt, J.A.: Intercellular adhesion and cancer invasion: a discrete simulation using the extended Potts Model. J. Theor. Biol. **216**, 85–100 (2002)
54. Aubert, M., Badoual, M., Grammaticos, B.: A model for short- and long range interactions of migrating tumor cells. Acta Biotheor. **56**, 297–314 (2008)
55. Barkey, P.D.: Structure and pattern formation in electrodeposition. In: Alkire, R.C. (ed.) Advances in Electrochemical Science and Engineering, pp. 151–192. J. Wiley-VHC-Verlag, New York, Frankfurt a/M (2001)
56. Angelini, T.E., Hannezo, E., Trepat, X., Fredberg, J.J., Weitz, D.A.: Cell migration driven by cooperative substrate deformation patterns. Phys. Rev. Lett. **104**, 168104 (2010)
57. Murray, J.D.: Mathematical Biology: I. An Introduction. Springer-Verlag, Berlin (2002)
58. Okubo, A.: Diffusion and Ecological Problems. Springer-Verlag, Berlin (1980)
59. Aubert, M., Badoual, M., Christov, C., Grammaticos, B.: A model for glioma cell migration on collagen and astrocytes. J. R. Soc. Interface **5**, 75–83 (2008)
60. López, J.M., Cuerno, R.: Power spectrum scaling in anomalous kinetic roughening of surfaces. Physica. A **246**, 329–347 (1997)
61. Ramasco, J.J., López, J.M., Rodríguez, M.A.: Generic dynamic scaling in kinetic roughening. Phys. Rev. Lett **84**, 2199–2202 (2000)
62. Wio, H.S., Escudero, C., Revelli, J.A., Deza, R.R., de la Lama, M.S.: Recent developments on the Kardar–Parisi–Zhang surface-growth equation. Phil. Trans. R. Soc. A **369**, 396–411 (2011)
63. Wio, H.S., Revelli, J.A., Deza, R.R., Escudero, C., de la Lama, M.S.: KPZ equation: Galilean-invariance violation, consistency, and fluctuation-dissipation issues in real-space discretization. Europhys. Lett. **89**, 40008 (2010)
64. Sasamoto, T., Spohn, H.: One-dimensional Kardar-Parisi-Zhang equation: an exact solution and its universality. Phys. Rev. Lett. **104**, 230602 (2010)
65. Calabrese, P., Le Doussal, P.: Exact solution for the Kardar-Parisi-Zhang equation with flat initial conditions. Phys. Rev. Lett **106**, 250603 (2011)
66. Khanin, K., Nechaev, S., Oshanin, G., Sobolevski, A., Vasilyev, O.: Ballistic deposition patterns beneath a growing Kardar-Parisi-Zhang interface. Phys. Rev. E **82**, 061107 (2010)
67. Takeuchi, A.K., Sano, M.: Universal fluctuations of growing interfaces: evidence in turbulent liquid crystals. Phys. Rev. Lett. **104**, 230601 (2010)
68. Takeuchi, A.K., Sano, M., Sasamoto, T., Spohn, H.: Growing interfaces uncover universal fluctuations behind scale invariance. Sci. Rep. **1**, 34 (2011). doi:10.1038/srep00034
69. Takeuchi, A.K., Sano, M.: Evidence for geometry-dependent universal fluctuations of the Kardar-Parisi-Zhang interfaces in liquid crystal turbulence. J. Stat. Phys. **147**, 853–890 (2012)